Agricultural and Forest Meteorology 338 (2023) 109518

Contents lists available at ScienceDirect

Agricultural and Forest Meteorology

journal homepage: www.elsevier.com/locate/agrformet

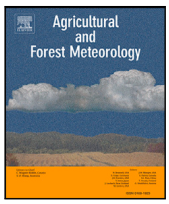

Inconsistency and correction of manually observed ground surface temperatures over snow-covered regions

Bin Cao [a], Shengdi Wang [b,*], Jiansheng Hao [c,*], Wen Sun [b], Kun Zhang [d,e]

[a] Key Laboratory of Tibetan Plateau Earth System, Environment and Resources (TPESER), National Tibetan Plateau Data Center (TPDC), Institute of Tibetan Plateau Research, Chinese Academy of Sciences, Beijing, 100101, China
[b] Key Laboratory of Western China's Environmental Systems (Ministry of Education), College of Earth and Environmental Sciences, Lanzhou University, Lanzhou, 730000, China
[c] Key Laboratory of Land Surface Pattern and Simulation, Institute of Geographic Sciences and Natural Resources Research, Chinese Academy of Sciences, Beijing, 100101, China
[d] Department of Mathematics, The University of Hong Kong, 999077, Hong Kong, China
[e] School of Biological Sciences, The University of Hong Kong, 999077, Hong Kong, China

ARTICLE INFO

Keywords:
Ground surface temperature
Snow cover
Snow insulation
Numerical simulation

ABSTRACT

Ground surface temperature (T_s) was manually measured using mercury thermometers in the early stage, and the snow surface temperature was substituted for T_s in areas with thick seasonal snow covers due to measurement difficulty. However, this practice produced T_s data that were inconsistent with more recent automatic measurements that determine T_s in the soil beneath the snow cover using modern instrumentation. In this study, we used observations from northeastern China to explore and correct this T_s inconsistency. Our results showed that the inconsistency varies from a few degrees to tens of degrees depending on the snow conditions and time periods considered. This inconsistency between earlier and modern measurements can lead to the overestimation of soil temperature warming rates in recent decades. We remove the T_s inconsistency using a numerical model that considers the effect of snow insulation on ground surface temperatures. This approach provides a means to improve T_s records that have similarly switched from manual to automatic measurements, which is critical for soil and climate investigations.

1. Introduction

The soil thermal regime has significant influences on hydrological processes (Ge et al., 2011), ecosystem (Pregitzer et al., 2000), agriculture, terrain carbon cycle (Curiel Yuste et al., 2007), and various temperature related phenomena (Cao et al., 2020). Soil thermal regime is generally dominated by large-scale climate conditions and refined by local-scale factors, such as soil moisture (Zwieback et al., 2019), vegetation cover, and seasonal snow cover (Cao et al., 2019a). Soil temperature is hence among one of the best indicators of terrain climate variability.

Long-term records of soil temperature, especially the ground surface temperature (T_s) in cold climates, are scarce in comparison to atmospheric measurements. This is primarily due to two reasons: (i) historical T_s measurements were manually conducted, and extreme cold environmental conditions made it difficult to access the areas, and (ii) the presence of snow cover added further challenges to T_s measurements. For these reasons, the World Meteorological Organization (WMO) suggests that measuring the temperature of the snow surface is desirable when the ground is covered with snow (Fig. 1A). This method (hereafter termed the manual protocol, T_s^m) represents the land surface temperature (LST) rather than T_s. T_s is collected automatically in the modern system (hereafter T_s^a) typically with a higher temporal resolution. By comparison, T_s^a in modern protocols is usually measured beneath the surface snow cover (Fig. 1B).

The manual protocol was generally followed for T_s measurements obtained from the meteorological station networks in the former Soviet Union (USSR) and China. Despite this, both sets of records are well organized and span a significant period, with the USSR record dating back to the 1890s and the Chinese record to the 1950s (Gilichinsky et al., 1998; Wang et al., 2015). These records have proven to be valuable for various research applications, including the study of land-atmosphere energy exchange (Zhang et al., 2018), changes in soil temperature (Streletskiy et al., 2015), investigations of near-surface soil freeze-thaw status (Wang et al., 2015), evaluation of remote-sensing data and products (Shao and Zhang, 2020), and detection of permafrost presence/absence (Cao et al., 2019b).

* Corresponding authors.
E-mail addresses: wangshd21@lzu.edu.cn (S. Wang), haojiansheng14@mails.ucas.ac.cn (J. Hao).

https://doi.org/10.1016/j.agrformet.2023.109518
Received 20 November 2022; Received in revised form 10 May 2023; Accepted 13 May 2023
Available online 27 May 2023

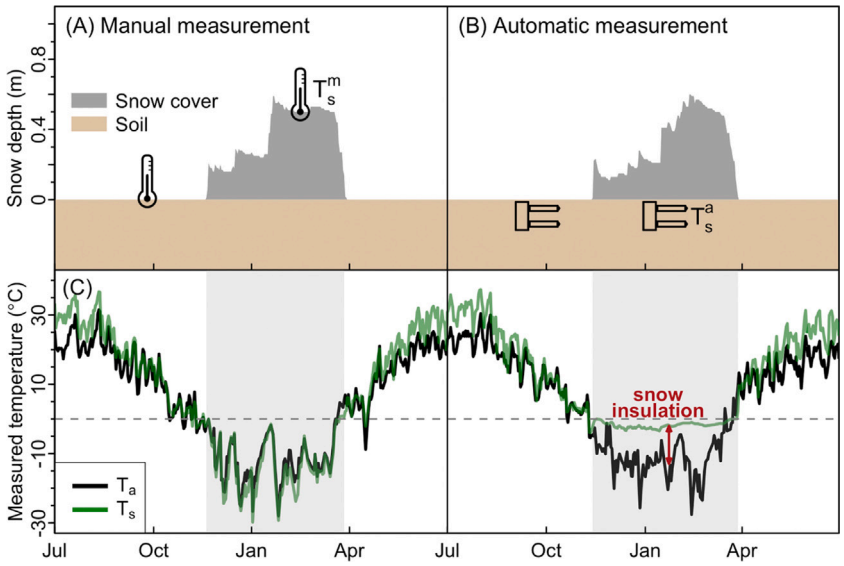

Fig. 1. Schematic illustration of ground surface temperature (T_s) measurement methods and comparisons of near-surface air temperature (T_a) and T_s. (A) Manual- (T_s^m) and (B) automatic-based (T_s^a) ground surface temperature measurements when seasonal snow layer is absent and present. (C) A time-series example of T_a and T_s obtained by different methods from Altay (88.08°E, 47.73°N).

The significant influences of seasonal snow cover on the soil thermal regime have been extensively investigated both in the field and through numerical experiments (Zhang, 2005; Slater et al., 2017; Cao et al., 2022). Depending on temporal scales, atmospheric and snow conditions, T_s can be several to tens of degrees warmer than T_a and the snow surface temperature (Zhang, 2005; Raleigh et al., 2013). This is often known as the snow-related surface offset in permafrost investigations (Hasler et al., 2014). In this case, a crucial issue arises: T_s obtained from the manual protocol is inconsistent with those commonly obtained using modern systems in cold regions when there is a snow cover. However, this issue has been ignored in some applications, such as Frauenfeld et al. (2004) and Streletskiy et al. (2015), or inaccurately interpolated as being consistent across T_s measurement methods (e.g., Wang et al., 2018; Song et al., 2022).

Since 2000, the routine manual ground surface temperature measurements were replaced by automatic systems using platinum resistance temperature sensors for the China Meteorological Administration (CMA) network (Cui et al., 2020). However, the datasets include the same variable name (i.e., T_s) for all measurements and do not include any correction to account for the change in measurement methodology. Due to this problem, there is an obvious inconsistency in T_s time-series observations from stations with seasonal snow cover, even though near-surface air temperature (T_a) is comparable (Fig. 1C). Recently, studies have reported on the inhomogeneity of observations from the CMA network and the possible impacts on climate research from an LST perspective (i.e., Cui et al., 2020; Du et al., 2020). However, the uncertainties in T_s are largely unknown and remain uncorrected.

In this study, we (i) report the inconsistency between T_s measurements made with the manual protocol *vs*. modern measurements, using the CMA datasets as an example, and (ii) quantify the magnitude of the T_s inconsistency (ΔT) attributed to the insulating effect of snow cover. We then (iii) discuss possible uncertainties in the T_s applications without considering the inconsistency, and (iv) provide a numerical method to remove the T_s inconsistency by converting snow surface temperature to ground surface temperature.

2. Study area and observations

Although the inconsistency of manually observed T_s is anticipated in all regions following the manual protocol (i.e., Russia, China, Mongolia, Kyrgyzstan and Tajikistan), we have selected the Tien Shan Mountains (TSM) in northwestern China as the study area. This area includes both snow-covered and snow-free stations in winter (Fig. 2). TSM, known as the a climatic transition zone, is dominated by cold Siberian air masses and westerly winds. The CMA daily observations, including: T_s, T_a and snow depth, from 87 meteorological stations, are used here to explore T_s inconsistency and evaluate the correction method. T_s was manually measured by professional technicians at 2:00, 8:00, 14:00, and 20:00 (UTC+8) in the manual system (Wang et al., 2015), and then is obtained using platinum resistance thermometer in the automatic system (Fig. 1) (Cui et al., 2020). The snow depth was measured daily at 8:00 (UTC+8) using a snow ruler in the manual observation system and using an ultrasonic or a laser snow depth measurement sensor with a typical accuracy of 1 cm in recent automatic system. The air pressure was measured using barographs or aneroid barometers in the manual system and then was changed to the resonator barometers in the automatic system. Wind speed was measured using electric anemometer. The measured mean annual air temperature ranged between −3.3 to 15.6 °C at the stations during the period of 1981–2010.

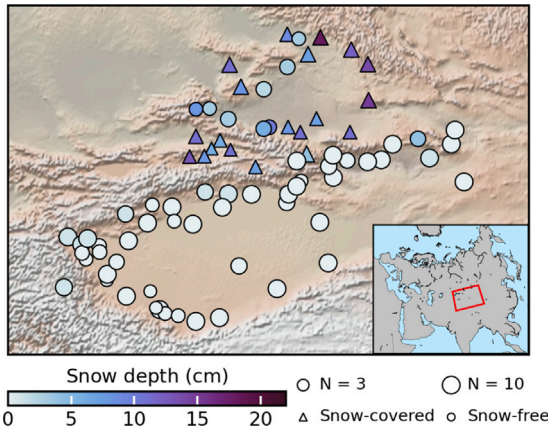

Fig. 2. Study area and the distribution of stations from China Meteorological Administration. The point size refers to the number of annual snow depth observations (N) during the period of 1999–2011.

We determined ΔT, i.e., soil temperature difference caused by inconsistent measurement methods, using T_s measurements from 5-years

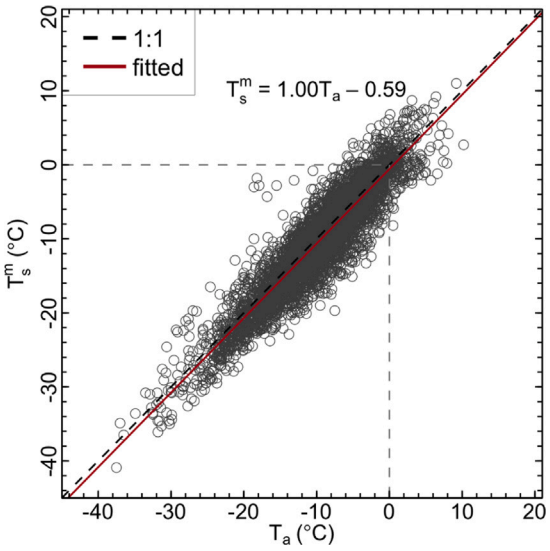

Fig. 3. Comparison of manually observed ground surface temperature (T_s^m) and near-surface air temperature (T_a) in snow-covered season from 1999 to 2004.

before and after the change from manual to automatic observations. During this period, we assume that (i) the general climate (e.g., radiation) and surface conditions (e.g., soil moisture) did not change significantly within that a short period, and (ii) ΔT is dominated by the changes in measurement methods due to the snow insulation effect. In this case, the observed T_s inconsistency (ΔT^o) is:

$$\Delta T^o = T_s^m - T_s^a \quad (1)$$

Site-specific information on when the measurement methods were switched was not available for this study, and therefore, it was visually determined for each snow-covered site. Fig. 1C provides an example showing the clear jump in T_s that occurs after a station is automated. The T_s^m is markedly cooler compared to T_s^a under similar T_a and snow conditions. Additional examples are shown in Fig. 8A and B, indicating that the switch between manual and automated measurements can be reliably determined. The switch at snow-covered stations in TSM was around 2005–2006, therefore, the T_s^m and T_s^a are estimated from observations during July 1999 to June 2004 and during July 2006 to June 2011, respectively. Data from the transition period was not used, in order to avoid any discrepancies using the mixed measurements.

The 87 stations in the study area were divided into snow-covered sites and (nearly) snow-free sites (Fig. 2). Snow-covered stations were defined as having a median annual maximum snow depth greater than 0.2 m during the period 1999–2011. Monthly and seasonal mean values were calculated for sites with soil temperature measurement completeness greater than 90%. The nearest temporal interpolation was used to fill the snow depth data gap. Due to the high albedo of snow cover, the T_s^m was found to be close to T_a in snow-covered region with a simple linear relationship (Fig. 3). Therefore, the missing T_s^m in snow-covered period was filled using

$$T_s^m = T_a - 0.59, \quad if \quad HS > 0 \quad (2)$$

where HS is the snow depth in centimeter. The remained missing T_a was then filled using 2-m air temperature from ERA5-Land, which is reported to have good agreement in TSM (Cao et al., 2020). Observed wind speed and air pressure were used for model forcing (see Section 3.2) and the data gap was filled based on ERA5-Land. Snow-covered season was defined from October to March.

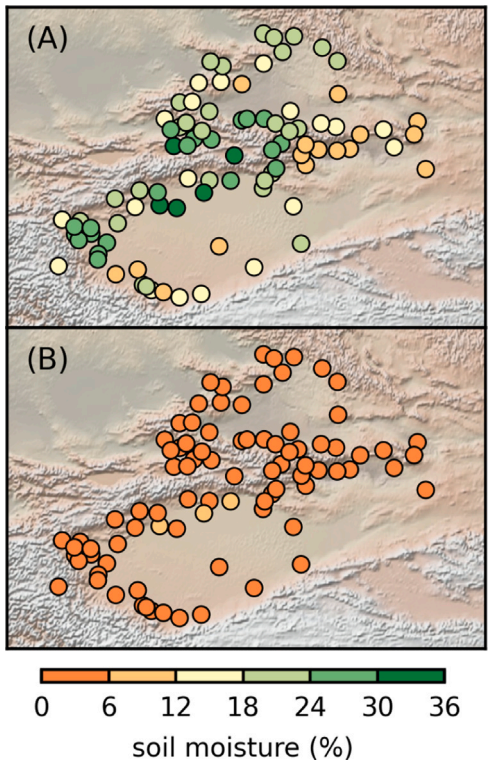

Fig. 4. (A) Mean and (B) standard deviation of ground surface soil moisture from May to September derived as ensemble of six remote-sensing products (2010–2018).

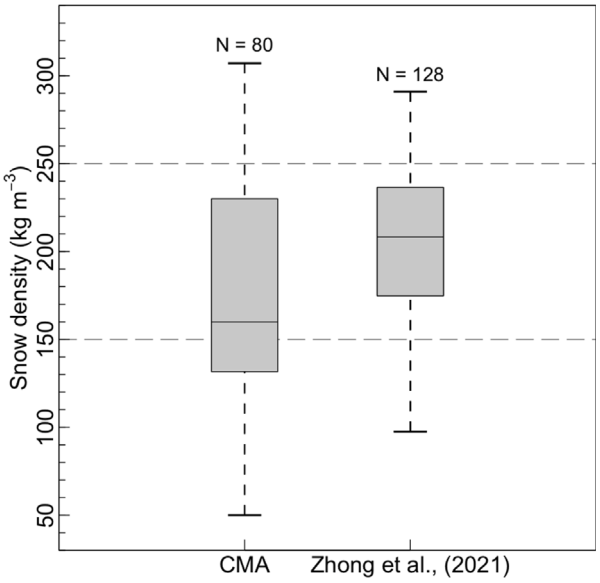

Fig. 5. Comparison of snow density from China Meteorological Administration and from the stand-along observations of Zhong et al. (2021). Only the datasets of 2015–2017 are used for China Meteorological Administration to align the measured period of stand-along observations. N is the sample number in each box.

3. Ground surface temperature inconsistency removal

3.1. Numerical model

To maximize the value of long-term T_s records from CMA, we removed the T_s inconsistency that occurred during the manual observation period. To achieve this, we transferred T_s observations from the

land surface (refers to the surface of the snow during snow-covered periods) to the ground surface. A numerical model with transient heat transfer and surface energy balance was used to simulate T_s and to remove the ΔT. The model was originally proposed by Ling and Zhang (2004) and the snow effects were considered in the model by extending the heat conduction solution into the 5-layer snow cover and computing the surface heat balance components as well as the snow surface temperature. It should be noted that the model processes are largely simplified in order to improve its transferability and to avoid the requirement of any additional model forcing and inputs.

Following Westermann et al. (2016), the surface energy balance is given as

$$Q = (1-\alpha)SW_{in} + LW_{in} + LW_{out} + Q_h + Q_e + Q_c \quad (3)$$

where SW_{in} (W m^{-2}) and LW_{in} (W m^{-2}) are short-wave and long-wave incoming radiation, respectively. α is surface albedo, since T_s was measured at bare ground conditions in summer, it was set as 0.20 for snow-free period, and as the snow albedo when snow is present. Detailed descriptions of surface energy balance components including: outgoing long-wave (LW_{out}), turbulent exchange of sensible (Q_h) and latent heat (Q_e) can be found in Ling and Zhang (2004). Snow specific parameterizations were revised following Westermann et al. (2013). The snow thermal conductivity (λ_{sn}, W m^{-1} K^{-1}), volumetric heat capacity (C_{sn}, J m^{-3} K^{-1}), and albedo (α_s) were revised to be solely dependent on snow density (ρ_{sn}, kg m^{-3}) following Douville et al. (1995)

$$\lambda_{sn} = \lambda_i \cdot \left(\frac{\rho_s}{\rho_i}\right)^{1.88} \quad (4)$$

$$C_{sn} = C_i \cdot \left(\frac{\rho_s}{\rho_i}\right) \quad (5)$$

$$\alpha_{sn} = 1.0 - 0.247(0.16 + 110(\rho_s \times 10^{-3})^4)^{\frac{1}{2}} \quad (6)$$

where ρ_i is the ice density of 920 kg m^{-3}, λ_i is the ice thermal conductivity of 2.2 W m^{-1} K^{-1}, and C_i is the ice volumetric thermal capacity of 2.05 × 10^6 J m^{-3} K^{-1}.

Heat conduction in the snow layer (Q_c) and soil is given by Fourier's law

$$Q_c = -(T_{s0} - T_s)\left(\frac{HS}{\lambda_{sn}} + \frac{z_0}{\lambda_s}\right) \quad (7)$$

$$C\frac{\partial T_g}{\partial t} = \frac{\partial}{\partial x}\left(\lambda_{sn}\frac{\partial T_g}{\partial x}\right) \quad (8)$$

where T_{s0} is the snow surface temperature (°C) simulated from the surface energy balance; z_0 is set as 0.03 m corresponding to the diameter of mercury ball thermometer (Wang et al., 2015). λ_{sn} and λ_s is snow and soil thermal conductivity (W m^{-1} °C^{-1}); C is apparent volumetric heat capacity and volumetric heat capacity of the soil (J m^{-3} °C^{-1}); t is time of day. T_g is simulated top layer soil at depth of z_0 or 0.03 m, and is taken as simulated T_s (T_s^s).

The soil thermal conductivity and capacity are treated as a mixture volumetric fractions (θ) of soil mineral (m), water (w), ice (i) and air (a), and is parameterized following Cosenza et al. (2003)

$$\lambda_s = \left[\theta_m\sqrt{\lambda_m} + \theta_w\sqrt{\lambda_w} + \theta_i\sqrt{\lambda_i} + \theta_a\sqrt{\lambda_a}\right]^2 \quad (9)$$

For bare ground conditions, the soil constituents organic is set as zero, air content (θ_i) is set as 0.05. The numerical model assumes a constant water content, and is derived from an ensemble mean of remote-sensing products. Soil mineral thermal conductivity (λ_m) is set as 2.92 W m^{-1}K^{-1} for the bare ground (Ling and Zhang, 2004; Cao et al., 2019a). However, the sensitivity experiments indicate λ_m has minimal influences on simulated T_s at the shallow simulated depth of 0.03 m (not shown). Water (λ_w) thermal conductivity is set as 0.57 W m^{-1}K^{-1}.

When soil is frozen, the super-cooled water or unfrozen water is parameterized following Niu and Yang (2006). The soil heat capacity for the soil process that accounts for the latent heat of freezing and melting of water/ice is given as

$$C = C_v + L\frac{\partial \theta_w}{\partial T} \quad (10)$$

where L is the specific volumetric latent heat of fusion of water. C_v is volumetric heat capacity (J m^{-3} K^{-1}) simulated from volumetric fractions of soil

$$C_v = C_m\theta_m + C_w\theta_w + C_i\theta_i + C_a\theta_a \quad (11)$$

where C_m, C_w, C_i, C_a is the volumetric heat capacity for mineral, water, ice, and air.

The numerical model simulated ΔT (ΔT^s) is hence given as

$$\Delta T^s = T_s^m - T_s^s \quad (12)$$

3.2. Model forcing and setting

The model uses T_a, snow depth, wind speed, and air pressure data obtained from the CMA network as forcing. However, the long- and short-wave radiations were not available in the CMA network, and therefore, data from ERA5-Land reanalysis were used. This is because the ERA5-Land reanalysis is reported to be reliable in representing atmospheric components in our study area (Cao et al., 2019b). Soil moisture content required by the model is estimated from six satellite-based products during 2010–2018, including: Advanced SCATterometer (ASCAT), Advanced Microwave Scanning Radiometer 2 (AMSR2-JAXA), Soil Moisture Ocean Salinity (SMOS-BEC and SMOS-IC) and the Soil Moisture Active Passive (SMAP-L3) satellite missions and the Climate Change Initiative Soil Moisture (CCI SM, v04.7) product. The ensemble daily mean and the standard deviation of the six products during the thawing period from May to September were used to allow for meaningful variations (Fig. 4). We used 106 soil layers with a total depth of 10 m. A lower boundary condition of zero heat flux was used for the T_s simulation.

The snow density measurements from the CMA were systematically underestimated relative to the stand-alone observations (Fig. 5). This is believed to be attributed to the snow density being measured with a heavy snow gauge that comprises a steelyard measurement balance and a 5000 cm^3 tube-cutter in CMA (Seligman and Douglas, 1936; Kinar and Pomeroy, 2015). In such a case, the model uses a constant snow density ranging from 150 to 250 kg m^{-3} based on the stand-alone in situ measurements from Zhong et al. (2021). Combined with the soil moisture range, we produced simulation ensemble to allow for meaningful temporal variations and uncertainties. The first five years of observations were used to spin up the model by running it 20 times (100 years) before simulation and analyses were conducted.

3.3. Evaluation

The mean bias (BIAS) and root mean squared error (RMSE) were used for model evaluation.

$$BIAS = \frac{1}{N}\sum_{i=1}^{N}(T_s^s - T_s^a) \quad (13)$$

$$RMSE = \sqrt{\frac{\sum_{i=1}^{N}(T_s^s - T_s^a)^2}{N}} \quad (14)$$

where N is the total number of measurements.

4. Results

4.1. Inconsistent ground surface temperature measurements

The ground surface temperatures measured by both the manual and automatic methods were similar in the snow-free season, despite using different measurement methods. Therefore, no significant ΔT^o (−0.7

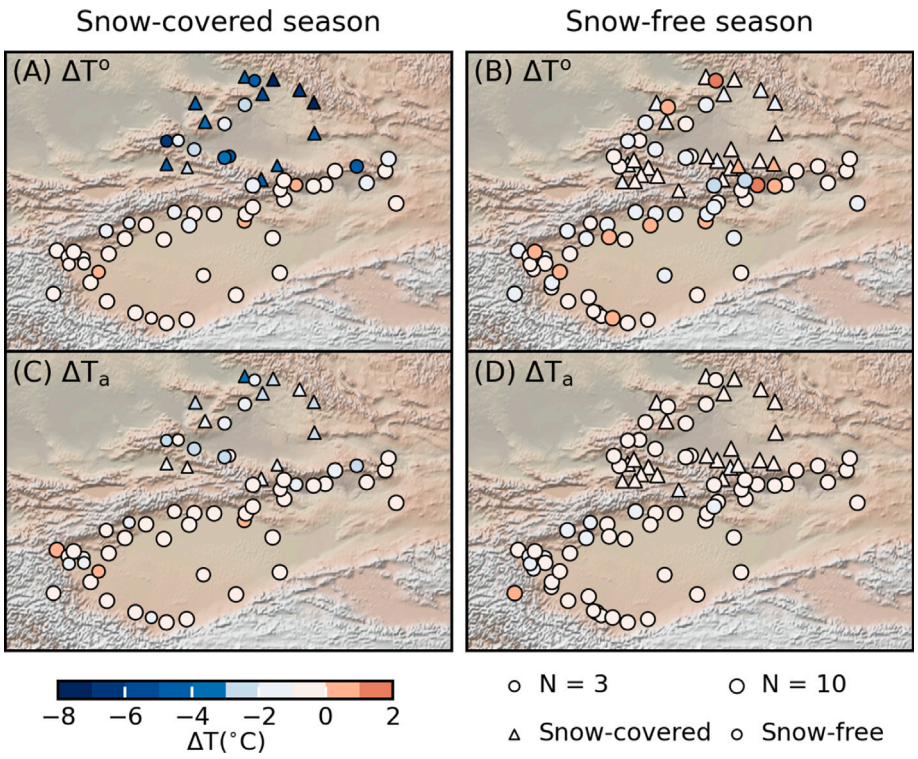

Fig. 6. Observed inconsistency (ΔT^o) of seasonal mean ground surface soil temperature between manual and automatic measurements during (A) snow-covered season (from October to March) and (B) snow-free season (April to September). Difference of mean near-surface air temperature (ΔT_a) between manual and automatic measurements in snow-covered (C) and snow-free (D) seasons. The manual measurement and automatic measurement are from the China Meteorological Administration (CMA) during 1999–2004 and 2006–2011, respectively. The point size refers numbers of observation (N).

± 0.7 °C) was found in the snow-free season (Fig. 6B). Conversely, during the snow-covered seasons from 1999–2011, the ΔT^o ranged from approximately −8.2 to 0.6 °C, despite a negligible difference in T_a, ranging from −3.3 to 0.3 °C (Fig. 6A and C). ΔT is closely related to snow depth, i.e., a larger snow depth typically leads to a greater ΔT (Figs. 2, 6A, 9B). Consequently, snow-covered stations had a mean seasonal ΔT^o of −5.0 ± 1.5 °C and a mean snow depth of 10 ± 3 cm from October to March, while there were no remarkable T^s differences at snow-free stations (−1.1 ± 1.4 °C). ΔT^o is more pronounced at a monthly scale. For example, the mean ΔT^o is −7.5 ± 2.2 °C with a mean snow depth about 20 ± 10 cm in January (Fig. 7A).

Similar to the spatial pattern, the temporal variation clearly shows the remarkable ΔT^o at stations with seasonal snow cover, although the T_a difference is minimal (Fig. 7). The aggregated monthly ΔT^o at the stations were as high as −8.0 to −6.5 °C in winter (DJF). By contrast, the change in measurement methodology generally had little influence on measured T_s in regions that are (nearly) free of snow (Fig. 7B), indicating that the remarkable ΔT is caused by inconsistent measurement methods.

4.2. Model evaluation

The modeled daily soil temperature at the ground surface (0.03 m) shows good agreement with the observations during both the snow-free and snow-covered seasons (Fig. 8). The RMSE of the simulated T_s in the snow-covered season was about 1.5–4.4 °C across annual to monthly timescales (Fig. 9A). Previous studies revealed that the temperature offset due to snow insulation at seasonal and monthly scales could be represented as a function of snow depth (HS) (Wang et al., 2016; Slater et al., 2017). Here we develop and estimate the model based on ΔT^s (Fig. 9B).

$$\Delta T = \begin{cases} -0.25 \cdot HS - 2.1, & if\ HS \le HS_{\text{eff}} \\ -10.9, & if\ HS > HS_{\text{eff}} \end{cases} \quad (15)$$

Table 1
The T_s trend (°C dec^{-1}) for original and ΔT removed (modeled) records at selected snow-covered sites with complete observations. The warming trend was estimated for two periods, i.e., since 1970 and 2000.

Data source	Annual	Snow-covered season	Snow-free season
	1970–2013		
Original	1.2	1.5	0.8
Modeled	0.8	0.8	0.8
	2000–2013		
Original	5.1	7.0	No trend
Modeled	No trend	No trend	No trend

where the HS_{eff} (cm) represents the snow depth threshold beyond which the insulation effect of snow is minimally affected by T_a variation. Since, HS_{eff} may vary depending on the near-surface atmospheric and snow conditions, it was set as 35 cm based on the observations from the Eurasian continent (Wang et al., 2016). The predictor is statistically significant in the fitted results ($P < 0.01$), and is in close agreement with the observed ΔT (with an RMSE of 1.5 °C), indicating the model is suitable for removing ΔT. The estimated negative intercept of −2.1 °C means that the thermal properties of the soil, soil phase change, and imperfect heat transfer between the ground surface and snow surface likely leads to an offset even if a seasonal snow layer is absent (Slater et al., 2017). Our results indicated the numerical model is suitable for the correction of manually measured ground surface temperature.

4.3. Ground surface temperature correction

T_s^m was cooler in snow-covered regions relative to T_s^a. As a consequence, T_s shows a more dramatic warming rate with an artificial T_s jump during 2004–2006, or the time when the measurement method switched (Fig. 10). For example, the T_s warming rate for the simulated

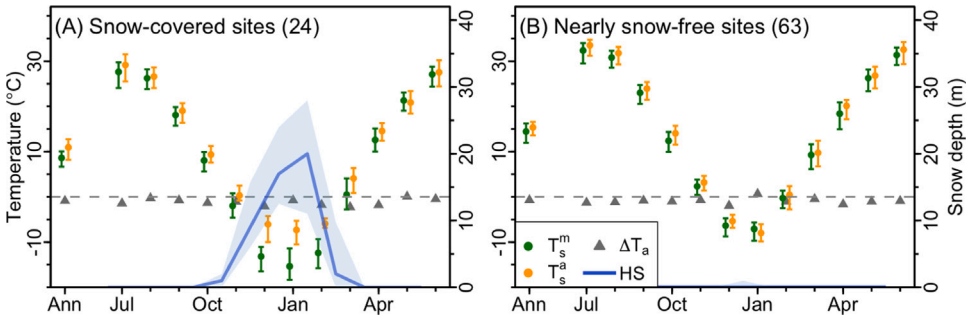

Fig. 7. Aggregated annual (Ann) monthly ground surface temperature from manual (T_s^m) and automatic (T_s^a) measurements at snow-covered (A) and (nearly) snow-free (B) sites. The snow depth (HS) and near-surface air temperature difference (ΔT_a) between manual and automated measurements are shown as the reference. The number of stations used for different measurements are given in the bracket.

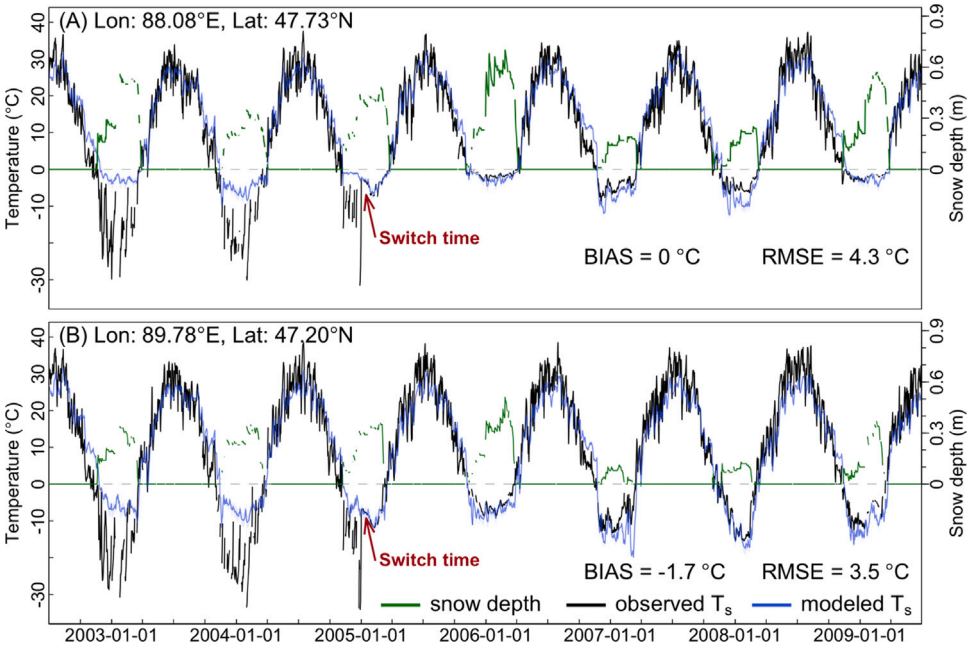

Fig. 8. Simulated daily T_s at two selected snow-covered stations.

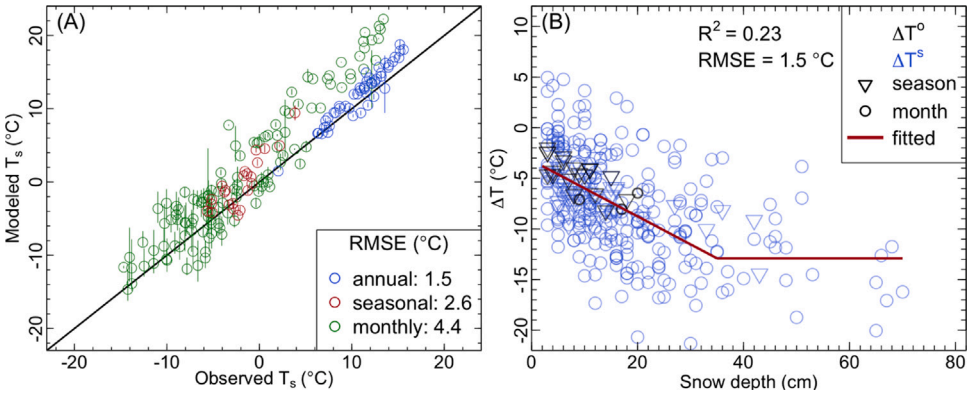

Fig. 9. (A) Comparison of modeled ground surface temperature (T_s^m) with observations at different temporal scales during the snow-covered season. (B) Relation between ΔT and snow depth at seasonal and monthly scales. The ensemble simulation depicts the spread between model runs with snow density and soil moisture content ranges with the ensemble mean (red line).

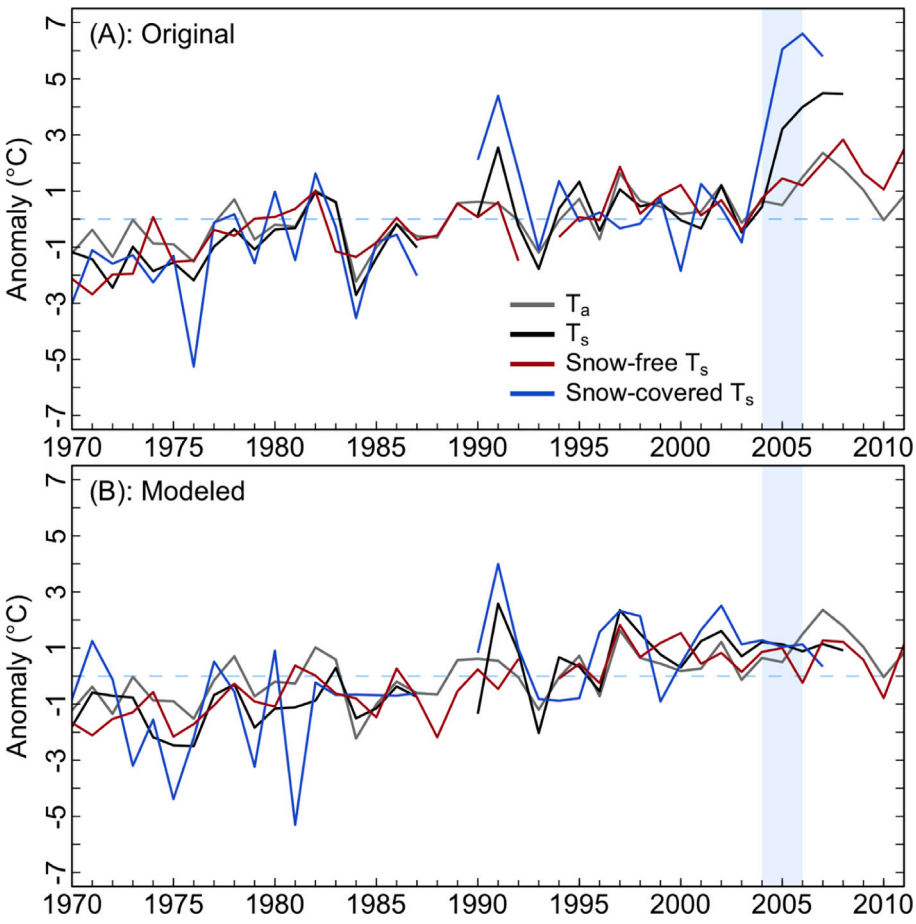

Fig. 10. The T_s trend for original and ΔT removed (modeled) records at selected snow-covered sites with complete observations. The bue shadow means the measurement switch period of 2004–2006.

T_s since 1970 was 0.8 °C dec^{-1} in the cold season and was 1.5 °C dec^{-1} for the observed data (Table 1). In contrast, T_s^m trend is comparable to T_s^s in the warm season and is similar to T_a. The remarkable ΔT in winter leads to a false annual T_s^m trend. For example, the observed rate of T_s change is warm biased by 0.35 °C dec^{-1} since 1970 compared to the modeled results (Table 1). The warming trend is overestimated to an even greater extent over shorter periods. For instance, the warming rate of T_s^m estimated since 2000 was about six times that estimated since 1970, while the simulated results show no trend (Table 1, Fig. 10).

5. Discussion

5.1. Simulation uncertainties

This study utilized numerical simulation to correct manually measured T_s, and carefully evaluated the results based on automatically measured T_s. To improve the model transferability and to reduce the dependency of model forcing, the physics in the model is largely simplified by mainly considering the most relevant processes of surface energy balance and heat transfer. We further acknowledge that many other processes, such as the absorption of shortwave radiation penetrating the snowpack (Kuipers Munneke et al., 2009), phase change within snow (Arduini et al., 2019), and aerodynamically smooth as well as aerodynamically rough conditions, may also have an important impact on the simulated T_s. In fact, the numerical uncertainties associated with the depth and time spacing could also be remarkable (Tubini et al., 2021). Additional uncertainties are likely attributed to the simplified assumption that the heat flux is zero at the 10 m depth and bias of radiation from ERA5-Land (Tang et al., 2021).

In this numerical simulation, we assumed constant soil moisture due to the small annual variation, i.e., standard deviation was about 2.2 ± 1.0% (Fig. 4B). Although the ensemble mean was used to improve representation, the soil moisture derived from remote-sensing is reported to have significant uncertainties (Gruber et al., 2020). This is expected to introduce possible uncertainties, which cannot be appropriately evaluated here due to lack of in-situ observations. In addition, the use of constant snow density with a reasonable variation may introduce additional uncertainties as snow density measurements were unrealistic. Previous studies have emphasized the significance of snow density in snow insulation on soil temperature (Zhang, 2005). Theretofore, future studies should consider using a state-of-the-art model that includes the evolution of snow density.

5.2. Insights

Previous studies suggested the snow surface temperature or land surface temperature over snow-covered regions could be estimated as a linear model of snow depth and solar radiation (e.g., Cui et al., 2020; Du et al., 2020). However, our findings indicated that the land surface temperature over snow-covered regions may be approximately equal to near-surface air temperature due to the high albedo of snow. As a result, we propose that long-term land surface temperature records could be estimated by combining ground surface temperature during the snow-free period and near-surface air temperature in the snow-covered period without the need for additional modeling.

The current numerical model, which considers surface energy balance and heat conduction processes, provides a practical and effective approach for simulating and correcting T_s at a site scale. While the

Table A.2
Definitions of symbols for this study.

Symbol	Name	Unit
T_s	Ground surface temperature	°C
T_a	Near-surface air temperature	°C
T_s^m	Manually measured ground surface temperature	°C
T_s^a	Automatically measured ground surface temperature	°C
ΔT	Soil temperature difference caused by inconsistent measurement methods	°C
ΔT^o	Observed soil temperature difference caused by inconsistent measurement methods	°C
ΔT^s	Simulated soil temperature difference caused by inconsistent measurement methods	°C
HS	Snow depth	m
HS_{eff}	Snow depth threshold beyond which snow insulation is little affected by air temperature	m
SW_{in}	Short-wave incoming radiation	W m^{-2}
LW_{in}	Long-wave incoming radiation	W m^{-2}
LW_{out}	Long-wave outcoming radiation	W m^{-2}
Q_h	Turbulent exchange of sensible heat	W m^{-2}
Q_e	Turbulent exchange of latent heat	W m^{-2}
Q_c	Conduction heat flux through the snow cover or ground surface	W m^{-2}
λ_{sn}	Snow thermal conductivity	W m^{-1} $°C^{-1}$
λ_i	Ice thermal conductivity	W m^{-1} $°C^{-1}$
λ_s	Soil thermal conductivity	W m^{-1} $°C^{-1}$
ρ_s	Soil density	kg m^{-3}
ρ_i	Ice density	kg m^{-3}
C	Thermal capacity of soil	J m^{-3} $°C^{-1}$
C_v	Volumetric heat capacity of soil	J m^{-3} $°C^{-1}$
C_{sn}	Thermal capacity of snow	J m^{-3} $°C^{-1}$
C_i	Thermal capacity of ice	J m^{-3} $°C^{-1}$
T_{s0}	Snow surface temperature	°C
Z_0	Depth of the top soil layer	m
λ_w	Soil thermal conductivity	%
g	Acceleration due to gravity	m s^{-2}
L	Specific volumetric latent heat of fusion of water	J

methods and solutions presented in this study were applied at a regional level in northeastern China, they are supposed to be applicable in other regions and countries that follow the manual measurement protocol estimated by the WMO, such as Mongolia, Kyrgyzstan, and Tajikistan. Consequently, the study is expected to provide useful information and insights for boarder regions and communities.

6. Conclusions

The manual protocol for measuring soil temperature has been extensively used worldwide, and long-term soil temperature observations are crucial for comprehending the changes in soil thermal state in response to global warming. In this study, we identified significant inconsistencies in ground surface temperature between historical manual measurements and modern measurements in snow-covered regions using CMA measurements. We also developed a method for removing inconsistency in historical manual records across large areas in China. This study provided valuable new insights that can be applied to future research on soil temperatures in cold regions:

(1) The ground surface temperatures obtained using the manual protocol are not consistent with modern measurements when there is seasonal snow cover. Prior to 2004 in the Tienshan Mountains, measurements were taken at the snow surface, while modem values (since 2006) were recorded from near the soil surface beneath the snow layer.
(2) Because of the significant impact of snow cover on the thermal regime of soil, the manual protocol-based measurements are cold biased and are incompatible with modern observations. As per the measurements taken by the China Meteorological Administration in the Tien Shan Mountains, there can be monthly differences of up to 20 °C.
(3) A solution for deriving consistent long-term soil temperature records is to use numerical models that account for the snow insulation effect. These models can transfer temperature from snow surface to ground surface and remove the T_s inconsistency.
(4) T_s warming rates reported without considering this inconsistency were over estimated due to the false T_s increase when the measurement methodology changed.

Declaration of competing interest

The authors declare that they have no known competing financial interests or personal relationships that could have appeared to influence the work reported in this paper.

Data availability

Data will be made available on request.

Acknowledgments

Authors would like to thank Daqing Yang and Hongqin Zhang for the helpful discussion and comments. We thank Xinyue Zhong for providing snow density observation datasets. This study was supported by the National Natural Science Foundation of China (NSFC) (grant no. 41988101, 42101134), the Second Tibetan Plateau Scientific Expedition and Research Program (STEP) (Grant No. 2019QZKK0903), Tibet Science and Technology Program (XZ202201ZY0011G), the Youth Innovation Promotion Association CAS (grant no: 2023075, to B. Cao), and the State Key Laboratory of Geodesy and Earth's Dynamics, China (grant no: SKLGED2023-5-1).

Appendix. Nomenclature

Table A.2 list provides the definitions of symbols for this study.

References

Arduini, G., Balsamo, G., Dutra, E., Day, J.J., Sandu, I., Boussetta, S., Haiden, T., 2019. Impact of a multi-layer snow scheme on near-surface weather forecasts. J. Adv. Modelling Earth Syst. 11 (12), 4687–4710. http://dx.doi.org/10.1029/2019MS001725, URL: https://onlinelibrary.wiley.com/doi/abs/10.1029/2019MS001725.

Cao, B., Arduini, G., Zsoter, E., 2022. Brief communication: Improving ERA5-land soil temperature in permafrost regions using an optimized multi-layer snow scheme. Cryosphere 16 (7), 2701–2708. http://dx.doi.org/10.5194/tc-16-2701-2022.

Cao, B., Gruber, S., Zheng, D., Li, X., 2020. The ERA5-land soil temperature bias in permafrost regions. Cryosphere 14, 2581–2595. http://dx.doi.org/10.5194/tc-14-2581-2020.

Cao, B., Quan, X., Brown, N., Stewart-Jones, E., Gruber, S., 2019a. GlobSim (v1.0): deriving meteorological time series for point locations from multiple global reanalyses. Geosci. Model Dev. 12, 4661–4679. http://dx.doi.org/10.5194/gmd-12-4661-2019.

Cao, B., Zhang, T., Wu, Q., Sheng, Y., Zhao, L., Zou, D., 2019b. Brief communication: Evaluation and inter-comparisons of Qinghai–Tibet plateau permafrost maps based on a new inventory of field evidence. Cryosphere 13, 511–519. http://dx.doi.org/10.5194/tc-13-511-2019.

Cosenza, P., Guerin, R., Tabbagh, A., 2003. Relationship between thermal conductivity and water content of soils using numerical modelling. Eur. J. Soil Sci. 54 (3), 581–588. http://dx.doi.org/10.1046/j.1365-2389.2003.00539.x.

Cui, J., Piao, S., Huntingford, C., Wang, X., Lian, X., Chevuturi, A., Turner, A.G., Kooperman, G.J., 2020. Vegetation forcing modulates global land monsoon and water resources in a CO2-enriched climate. Nature Commun. 11 (1), 1–11. http://dx.doi.org/10.1038/s41467-020-18992-7.

Curiel Yuste, J., Baldocchi, D.D., Gershenson, A., Goldstein, A., Misson, L., Wong, S., 2007. Microbial soil respiration and its dependency on carbon inputs, soil temperature and moisture. Global Change Biol. 13 (9), 2018–2035. http://dx.doi.org/10.1111/j.1365-2486.2007.01415.x.

Douville, H., Royer, J.F., Mahfouf, J.F., 1995. A new snow parameterization for the Météo-France climate model: Part I: validation in stand-alone experiments. Clim. Dynam. 12 (1), 21–35. http://dx.doi.org/10.1007/BF00208760.

Du, J., Wang, K., Cui, B., Jiang, S., 2020. Correction of inhomogeneities in observed land surface temperatures over China. J. Clim. 33 (20), 8885–8902. http://dx.doi.org/10.1175/JCLI-D-19-0521.1.

Frauenfeld, O.W., Zhang, T., Barry, R.G., Gilichinsky, D., 2004. Interdecadal changes in seasonal freeze and thaw depths in Russia. J. Geophys. Res. D: Atmos. 109 (5), 413–421. http://dx.doi.org/10.1029/2003jd004245.

Ge, S., McKenzie, J., Voss, C., Wu, Q., 2011. Exchange of groundwater and surface-water mediated by permafrost response to seasonal and long term air temperature variation. Geophys. Res. Lett. 38, 1–6. http://dx.doi.org/10.1029/2011GL047911.

Gilichinsky, D., Barry, R.G., Bykhovets, S.S., Sorokovikov, V., Zhang, T., Zudin, S.L., Fedorov-Davydov, D.G., 1998. A century of temperature observations of soil climate: methods of analysis and long-term trends. In: The 7th International Permafrost Conference. pp. 313–317.

Gruber, A., Lannoy, G.D., Albergel, C., Al-Yaari, A., Brocca, L., Calvet, J.-C., Colliander, A., Cosh, M., Crow, W., Dorigo, W., Draper, C., Hirschi, M., Kerr, Y., Konings, A., Lahoz, W., McColl, K., Montzka, C., Muñoz-Sabater, J., Peng, J., Reichle, R., Richaume, P., Rüdiger, C., Scanlon, T., van der Schalie, R., Wigneron, J.-P., Wagner, W., 2020. Validation practices for satellite soil moisture retrievals: What are (the) errors? Remote Sens. Environ. 244, 111806. http://dx.doi.org/10.1016/j.rse.2020.111806.

Hasler, A., Geertsema, M., Foord, V., Gruber, S., Noetzli, J., 2014. The influence of surface characteristics, topography, and continentality on mountain permafrost in British Columbia. Cryosphere Discuss. 8 (5), 4779–4822. http://dx.doi.org/10.5194/tcd-8-4779-2014.

Kinar, N.J., Pomeroy, J.W., 2015. Measurement of the physical properties of the snowpack. Rev. Geophys. 53 (2), 481–544. http://dx.doi.org/10.1002/2015RG000481.

Kuipers Munneke, P., van den Broeke, M.R., Reijmer, C.H., Helsen, M.M., Boot, W., Schneebeli, M., Steffen, K., 2009. The role of radiation penetration in the energy budget of the snowpack at summit, Greenland. Cryosphere 3 (2), 155–165. http://dx.doi.org/10.5194/tc-3-155-2009, URL: https://tc.copernicus.org/articles/3/155/2009/.

Ling, F., Zhang, T., 2004. A numerical model for surface energy balance and thermal regime of the active layer and permafrost containing unfrozen water. Cold Reg. Sci. & Technol. 38 (1), 1–15. http://dx.doi.org/10.1016/S0165-232X(03)00057-0.

Niu, G.-Y., Yang, Z.-L., 2006. Effects of frozen soil on snowmelt runoff and soil water storage at a continental scale. J. Hydrometeorol. 7 (5), 937–952. http://dx.doi.org/10.1175/JHM538.1.

Pregitzer, K.S., King, J.S., Burton, A.J., Brown, S.E., 2000. Responses of tree fine roots to temperature. New Phytol. 147, 105–115. http://dx.doi.org/10.1046/j.1469-8137.2000.00689.x.

Raleigh, M.S., Landry, C.C., Hayashi, M., Quinton, W.L., Lundquist, J.D., 2013. Approximating snow surface temperature from standard temperature and humidity data: New possibilities for snow model and remote sensing evaluation. Water Resour. Res. 49 (12), 8053–8069. http://dx.doi.org/10.1002/2013WR013958.

Seligman, G., Douglas, C.K.M., 1936. Snow Structure and Ski Fields: Being an Account of Snow and Ice Forms Met with in Nature, and a Study on Avalanches and Snowcraft. Macmillan.

Shao, W., Zhang, T., 2020. Assessment of four near-surface soil freeze/thaw detection algorithms based on calibrated passive microwave remote sensing data over China. Earth and Space Sci. 7, e2019EA000807. http://dx.doi.org/10.1029/2019EA000807.

Slater, A.G., Lawrence, D.M., Koven, C.D., 2017. Process-level model evaluation: a snow and heat transfer metric. Cryosphere 11 (2), 989–996. http://dx.doi.org/10.5194/tc-11-989-2017.

Song, P., Zhang, Y., Guo, J., Shi, J., Zhao, T., Tong, B., 2022. A 1-km daily surface soil moisture dataset of enhanced coverage under all-weather conditions over China in 2003–2019. Earth System Sci. Data 14 (6), 2613–2637. http://dx.doi.org/10.5194/essd-14-2613-2022.

Streletskiy, D.A., Sherstiukov, A.B., Frauenfeld, O.W., Nelson, F.E., 2015. Changes in the 1963–2013 shallow ground thermal regime in Russian permafrost regions. Environ. Res. Lett. 10 (12), 125005. http://dx.doi.org/10.1088/1748-9326/10/12/125005.

Tang, W., Qin, J., Yang, K., Zhu, F., Zhou, X., 2021. Does ERA5 outperform satellite products in estimating atmospheric downward longwave radiation at the surface? Atmos. Res. 252, 105453. http://dx.doi.org/10.1016/j.atmosres.2021.105453.

Tubini, N., Gruber, S., Rigon, R., 2021. A method for solving heat transfer with phase change in ice or soil that allows for large time steps while guaranteeing energy conservation. Cryosphere 15 (6), 2541–2568. http://dx.doi.org/10.5194/tc-15-2541-2021.

Wang, L., Henderson, M., Liu, B., Shen, X., Chen, X., Lian, L., Zhou, D., 2018. Maximum and minimum soil surface temperature trends over China, 1965–2014. J. Geophys. Res.: Atmos. 123 (4), 2004–2016. http://dx.doi.org/10.1002/2017JD027283.

Wang, W., Rinke, A., Moore, J.C., Ji, D., Cui, X., Peng, S., Lawrence, D.M., McGuire, A.D., Burke, E.J., Chen, X., Decharme, B., Koven, C., MacDougall, A., Saito, K., Zhang, W., Alkama, R., Bohn, T.J., Ciais, P., Delire, C., Gouttevin, I., Hajima, T., Krinner, G., Lettenmaier, D.P., Miller, P.A., Smith, B., Sueyoshi, T., Sherstiukov, A.B., 2016. Evaluation of air–soil temperature relationships simulated by land surface models during winter across the permafrost region. Cryosphere 10 (4), 1721–1737. http://dx.doi.org/10.5194/tc-10-1721-2016.

Wang, K., Zhang, T., Zhong, X., 2015. Changes in the timing and duration of the near-surface soil freeze/thaw status from 1956 to 2006 across China. Cryosphere 9, 1321–1331. http://dx.doi.org/10.5194/tc-9-1321-2015.

Westermann, S., Langer, M., Boike, J., Heikenfeld, M., Peter, M., Etzelmüller, B., Krinner, G., 2016. Simulating the thermal regime and thaw processes of ice-rich permafrost ground with the land-surface model CryoGrid 3. Geosci. Model Dev. 9 (2), 523–546. http://dx.doi.org/10.5194/gmd-9-523-2016.

Westermann, S., Schuler, T.V., Gisnås, K., Etzelmüller, B., 2013. Transient thermal modeling of permafrost conditions in southern Norway. Cryosphere 7 (2), 719–739. http://dx.doi.org/10.5194/tc-7-719-2013.

Zhang, T., 2005. Influence of the seasonal snow cover on the ground thermal regime: An overview. Rev. Geophys. 43 (4), RG4002. http://dx.doi.org/10.1029/2004RG000157.

Zhang, H., Zhang, F., Zhang, G., Che, T., Yan, W., 2018. How accurately can the air temperature lapse rate over the tibetan plateau be estimated from MODIS LSTs? J. Geophys. Res.: Atmos. 1–18. http://dx.doi.org/10.1002/2017JD028243.

Zhong, X.Y., Zhang, T., Su, H., Xiao, X.X., Wang, S.F., Hu, Y.T., Wang, H.J., Zheng, L., Zhang, W., Xu, M., Wang, J., 2021. Impacts of landscape and climatic factors on snow cover in the altai mountains, China. Adv. Clim. Chang. Res. 12 (1), 95–107. http://dx.doi.org/10.1016/j.accre.2021.01.005.

Zwieback, S., Westermann, S., Langer, M., Boike, J., Marsh, P., Berg, A., 2019. Improving permafrost modeling by assimilating remotely sensed soil moisture. Water Resour. Res. 55 (3), 1814–1832. http://dx.doi.org/10.1029/2018WR023247.